Comparison of Geometrically Shaped 32-QAM and Probabilistically Shaped 32-QAM in a Bandwidth-Limited IM-DD System

Junjie Ding, Jiao Zhang, Yiran Wei, Feng Zhao, Chaoyang Li, Jianjun Yu*, Fellow, IEEE, Fellow, OSA

***Abstract*— We use the generalized pair-wise optimization (PO) algorithm to optimize the geometrically shaped 32-ary quadrature amplitude modulation (GS-32-QAM) constellation and adopt the probabilistic fold shaping (PFS) scheme to generate the probabilistically shaped 32-QAM (PS-32-QAM) format. We present a detailed comparison among the application of GS-32-QAM, PS-32-QAM and uniform 32-QAM in an intensity modulation/direct detection (IM/DD) system with a bandwidth-limited digital-to-analog converter (DAC). We experimentally demonstrate the 32-QAM discrete Fourier transform-spread (DFT-S) discrete multi-tone (DMT) signal transmission over 1-km standard single mode fiber (SSMF) in an IM/DD system with a net data rate of 108.29-Gb/s/λ, and achieve 0.6 dB and 0.9 dB receiver sensitivity gain using PS and GS constellations, respectively. In the high signal to noise ratio (SNR) case with a net bit rate of 69.61-Gb/s/λ, the PS-32-QAM DMT signal can provide the receiver sensitivity gain of 0.5 dB while the receiver sensitivity gain of the GS-32-QAM DMT signal is 0.4 dB, compared to the uniform 32-QAM DMT signal. Although PS-32-QAM achieves better receiver sensitivity gain than GS-32-QAM in the high SNR case, the proposed GS-32-QAM format outperforms PS-32-QAM in the low SNR case.**

***Index Terms*—Probabilistic shaping, geometric shaping, intensity modulation/direct detection (IM/DD), discrete multi-tone (DMT).**

This work is supported by the Chinese National key R&D projects under grant number 2018YFB1800900, National Natural Science Foundation of China under Grants 61935005, 91938202, 61922025 61527801, 61675048, 61720106015, 61835002, 61875164, and 61805043. (*Corresponding author: Jianjun Yu*.)

J. Ding, J. Zhang, Y. Wei, and J. Yu are with Shanghai Institute for Advanced Communication and Data Science, Key Laboratory for Information Science of Electromagnetic Waves (MoE), and State Key Laboratory of ASIC and System, Fudan University, Shanghai 200433, China (e-mail: 18110720017@fudan.edu.cn; 17110720046@fudan.edu.cn; 18110720055@fudan.edu.cn; jianjun@fudan.edu.cn).

F. Zhao is with Xian University of Posts and Telecommunications, Xian, 710121, China (email: hfengzhao@xupt.edu.cn).

C. Li is with Department of Engineering and Computer Science, Oakland University, Rochester, Michigan, 48309, USA (email: chaoyangli@oakland.edu).

I. Introduction

Since the emergence of information theory, narrowing the gap between the system capacity and Shannon limit has become a focus in the field of communication. In order to meet the requirement of high capacity and high spectral efficiency transmission in optical fiber communication system, 16-ary quadrature amplitude modulation (16-QAM), 64-QAM and other higher-order traditional rectangular QAM formats have been widely used. However, the traditional rectangular QAM constellation cannot effectively increase the communication system capacity and transmission distance because its minimum Euclidean distance is not optimized. Therefore, constellation shaping techniques need to be applied to the optical communication system.

Probabilistic shaping technique can effectively alleviate the nonlinear effects of signals in the optical channel [1-2], obtain a flexible data rate and improve the system capacity [3-5], where QAM constellation points satisfy the Maxwell-Boltzmann distribution by utilizing a distribution matcher (DM). P. Schulte and G. Böcherer proposed a practical, invertible and fixed-to-fixed length distribution matcher called constant composition distribution matcher (CCDM), which is robust to synchronization and variable rate problems [6-8]. However, CCDM adopts the many-to-one mapping method and requires iterative de-mapping, therefore, suffers from high computational complexity for probabilistically shaped (PS) QAM generation.

On the other hand, the geometric shaping technique exploits the non-uniformly spaced constellation distribution with a larger minimum Euclidean distance to make the system capacity closer to the Shannon limit [9-13]. Different schemes have been proposed to design geometrically shaped (GS) constellations. Monte Carlo (MC) simulation algorithm can be used to maximize the minimum Euclidean distance for geometric shaping. However, it has high computational complexity for high-order QAM format. In Ref. 14, the pair-wise optimization (PO) algorithm was proposed to optimize GS constellation for non-uniform sources. A generalized PO algorithm based on the minimization of the analytical bit error rate (BER) of given constellation points and bits mapping was proposed in Ref. 15 to design multi-dimensional modulation formats. In addition, A new geometric shaping scheme was introduced in Ref. 16 to

optimize the signal constellation by maximizing the generalized mutual information (GMI) of binary and non-binary codes.

In recent years, the geometric shaping technique has been applied in the high-speed optical fiber communication system [17-18] and has become an important development direction of 1Tb/s signal transmission. In Ref. 19, a code modulation method combined with probabilistic shaping and geometric shaping is used to achieve 70.4 Tb/s information transmission over 7600 km on the C + L band experimentally.

Meanwhile, the comparison of probabilistic shaping and geometric shaping has been widely concerned and discussed [20-21]. In Ref. 20, it has been proved that probabilistic shaping enables seamless rate adaptation and outperforms ATSC 3.0 geometric shaping by more than 0.5 dB for spectral efficiencies larger than 3.2 bits per channel in the additive white Gaussian noise (AWGN) channel. Ref. 21 has compared the performance of GS-QAM and PS-QAM constellations with that of regular square QAM modulation. The proposed geometric shaping with bit-interleaved coded modulation (BICM) architecture can achieve good performance gains and maintain low complexity, while probabilistic shaping obtains superior performance but has high computational complexity.

Orthogonal frequency division multiplexing (OFDM) has been widely used due to its high spectrum efficiency and tolerance for inter-symbol interference (ISI) and inter-carrier interference (ICI). Discrete Fourier transform-spread (DFT-S) discrete multi-tone (DMT) is adopted to generate real-value baseband transmitted signal with low peak to average power ratio (PAPR) [22-24].

Most of the previous works carry out the experimental comparison between PS-QAM and GS-QAM in single carrier modulation with coherent detection. However, the comparison between PS-QAM and GS-QAM with DMT modulation in an intensity modulation/direct detection (IM/DD) system with bandwidth-limited devices is of great value, considering the requirements of low cost in interconnect applications. A 108.29-Gb/s/λ 32-QAM DFT-S DMT over 1-km standard single-mode fiber (SSMF) is experimentally demonstrated in a cost-effective IM/DD system with a bandwidth-limited digital-to-analog converter (DAC). With the increase of signal bandwidth, severe power fading occurs in high frequency edge due to the roll-off effect of DAC. Therefore, signal to noise ratio (SNR) degrades due to less effective number of bits (ENOB) and weaker frequency response at high frequencies of the DAC. In this paper, GS-32-QAM and PS-32-QAM are compared in both low SNR and high SNR cases. Optimized GS constellation is applied in the IM-DD system which achieves 0.9 dB receiver sensitivity gain and outperforms PS-32-QAM in the low SNR case. However, in the high SNR case, PS-32-QAM outperforms GS-32-QAM by more than 0.1 dB in receiver sensitivity.

The rest of this paper is organized as follows. The principles of GS, PS and DFT-S DMT format are described in Section II. Section III illustrates the experimental setup of the GS-32-QAM DFTS-DMT system. Section IV evaluates the experimental performance and discusses the results. Finally, a conclusion is provided in Section V.

II. Principle and Analysis

In this section, we present the principles of geometric shaping, probabilistic shaping and DFT-S DMT format. We demonstrate the optimized constellation of GS-32-QAM with the generalized PO algorithm over an AWGN channel and the block diagram of PS-32-QAM generation.

A. Geometric Shaping

We optimize constant-power GS constellations by the generalized PO algorithm with simplified calculations [15]. To facilitate this optimization process, we first have to minimize the symbol error rate (SER) which depends on the location of the constellation points. Then, we find the mapping of the optimum bits to minimize the BER and GMI. But if the bits mapping and SNR are given, we just have to minimize the analytical BER equation which can efficiently simplify the optimization problem.

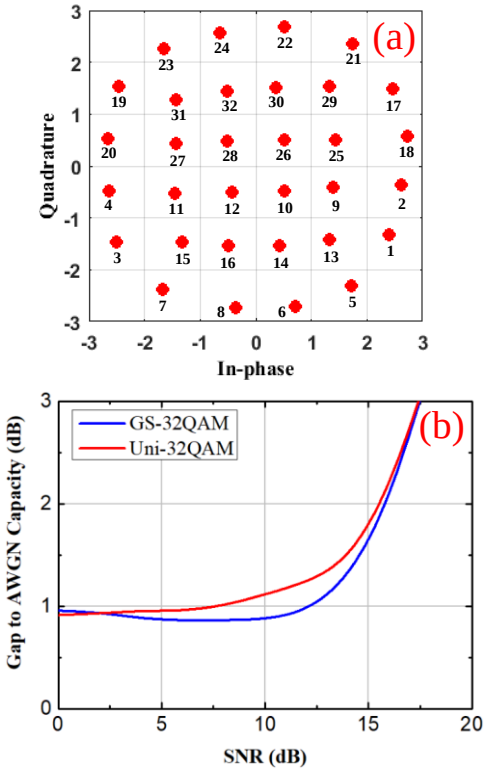

Fig. 1 (a) Constellation of GS-32-QAM based on generalized PO algorithm. (b) Gap to capacity assuming an AWGN channel.

Considering M-QAM format in a two-dimensional constellation, there are M symbols $\{\boldsymbol{s}_1, \boldsymbol{s}_2, \cdots, \boldsymbol{s}_M\}$ with equal probability. Symbol $\boldsymbol{s}_k, k \in \{1, 2, \cdots, M\}$ is a 2×1 vector and consist of in-phase and quadrature components. It contains $\log_2 M$ bits, the bit mapping of which is expressed as B_k. The Hamming distance $h(B_k, B_l)$ represents the number of different bits encoded between symbols $\boldsymbol{s}_k$ and $\boldsymbol{s}_l$, which is used to convert the SER to BER.

The analytical SER upper bound is formulated as:

$$Q\left(\frac{\|\boldsymbol{s}_k-\boldsymbol{s}_l\|}{\sqrt{2N_0}}\right) \tag{1}$$

where $Q(x)=\frac{1}{\sqrt{2\pi}}\int_x^{\infty}e^{-y^2/2}dy$ refers to the Gaussian Q-function, and $\|\cdot\|$ represents the norm operation of a vector. The Gaussian noise variance is N_0 which is calculated by the given SNR. Finally, the analytical BER expression to be minimized can be given out as follows:

$$\frac{1}{M}\sum_{k=1}^{M}\sum_{l=1,l\neq k}^{M}h(B_k,B_l)\cdot Q\left(\frac{\|\boldsymbol{s}_k-\boldsymbol{s}_l\|}{\sqrt{2N_0}}\right) \tag{2}$$

$$\text{subject to}\ \sum_{k=1}^{M}\boldsymbol{s}_k=0\ \text{ and }\ \sum_{k=1}^{M}\|\boldsymbol{s}_k\|^2=M \tag{3}$$

Our objective is to optimize the arrangement of the points in initial M-ary constellation to minimize the analytical BER equation at a given SNR. The optimization process is repeated until the maximum number of iterations is reached or the optimized performance improvement is saturated.

Fig. 1(a) shows the optimized constellation of GS-32-QAM with the generalized PO algorithm over an AWGN channel with a fixed SNR of 12 dB. The gap to AWGN capacity of GS-32-QAM and uniform 32-QAM is shown in Fig. 1(b), which is defined as: $SNR_{dB}-10\log_{10}(2^{GMI}-1)$. It indicates that GS-32-QAM can obtain ~0.3 dB gain for an SNR of 12 dB.

B. Probabilistic Shaping

The probability distribution of each constellation point in PS-QAM format follows the Maxwell-Boltzmann distribution, which is written as:

$$P_X(x_i)=\frac{1}{\sum_{k=1}^{M}e^{-vx_k^2}}e^{-vx_i^2} \tag{4}$$

where v is a scaling factor that can be adjusted to change the information entropy and achieve rate-adaptation.

A probabilistic amplitude shaping (PAS) scheme proposed in Ref. 7 is used to achieve PS M^2-order QAM symbols. However, it can only be used for square QAM formats and is not applicable to 32-QAM format. Here we adopt the probabilistic fold shaping (PFS) scheme in Ref. 25, which can be used for N-fold rotationally symmetrical QAM formats and suitable for the 4-fold symmetrical 32-QAM.

The block diagram of PS-32-QAM generation according to the principle of the PFS scheme is shown in Fig. 2. Firstly, the binary data stream is divided into two branches consisting of U_1 and U_2 bits. U_1 bits on the upper branch are transformed into CCDM module to obtain V_1 symbols with the desired Maxwell-Boltzmann distribution. Thus, the rate of CCDM is $R_{DM}=U_1/V_1$. Non-uniformly distributed symbols are achieved after the DM and mapped to eight constellation points in one-fold/quadrant with different colors which indicate different probabilities. Subsequently, each symbol is expressed by a binary label with 3 bits. $3V_1$ bits converted from V_1 non-uniformly distributed symbols and U_2 uniformly distributed original bits from the lower branch are concatenated together and encoded with LDPC. After encoder, a sequence of uniformly distributed parity check bits can be obtained. Then, these parity check bits combined with U_2 information bits are used as fold index bits which gives the symmetry for the symbol mapping. Meanwhile, $3V_1$ information bits converted from non-uniformly distributed symbols are used as amplitude bits. Finally, fold index bits and amplitude bits are combined and transformed into a sequence of symbols with Maxwell-Boltzmann distribution to generate the PS-32-QAM format.

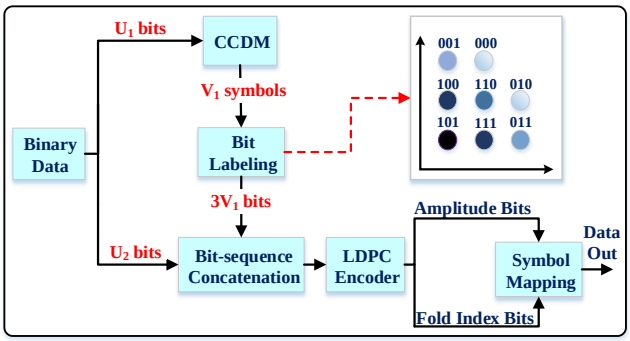

Fig. 2. Block diagram of PS-32-QAM generation.

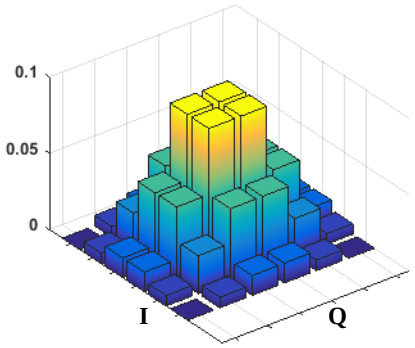

Fig. 3. The constellation of the probability distributions for PS-32-QAM. The bars represent the probability for each symbol.

Here we set the scaling factor v as 0.081, and thus the entropy of PS-32-QAM is 4.5 bits/symbol. The corresponding probability distributions for the constellation of PS-32-QAM format are illustrated in Fig. 3.

The theoretical transmission rate, *R*, is calculated by

$$R=H-m\cdot(1-r) \tag{5}$$

where *H* is entropy, *m* is the number of bits per symbol of the QAM constellation, *r* is forward error correction (FEC) code rate. Considering a given FEC code rate of 9/10, the calculated transmission rate R of PS-32-QAM is thus 4.5-5× (1-9/10) =4 b/s. When we need to generate V_1=81920 PS-32-QAM symbols, U_1 and U_2 should be 204549 and 122880. The rate of CCDM is $R_{DM}=U_1/V_1=2.5$. The transmission rate can also be calculated by $(U_1+U_2)/V_1$, which is equal to 4 b/s.

C. DFT-S DMT Format

The block diagram of DFT-S DMT system is shown in Fig. 4. The DMT signal is generated off-line. The data is first mapped into the designed GS-32-QAM, PS-32-QAM or uniform 32-QAM. Then, DFT-S is added to suppress PAPR of DMT signal. We use N low positive frequency subcarriers loaded

with data for additional N-point DFT. Pre-equalization is implemented to compensate for high frequency power attenuation. Another N low negative frequency subcarriers carry Hermitian symmetric data after the pre-equalization. The first subcarrier is set to zero in the input of 8192-point inverse fast Fourier transform (IFFT) for DMT signal generation. One training sequence (TS) in 32 DFT-S DMT symbols is used to estimate the channel. 16-sample cyclic prefix (CP) is added to avoid the ISI before the parallel to serial conversion. Here, to obtain PS-32-QAM DMT signal with 25-GHz bandwidth, the N should be 25/80×8192=2560. The net bit rate is thus 25×4×8192/ (8192+16) ×31/32=96.69-Gb/s.

The off-line digital signal processing (DSP) includes CP removal, serial to parallel conversion, 8192-point fast Fourier transform (FFT), channel estimation with intra-symbol frequency-domain averaging (ISFA), N-point IFFT, direct-detection least mean square (DD-LMS), 32-QAM de-mapping and GMI calculation.

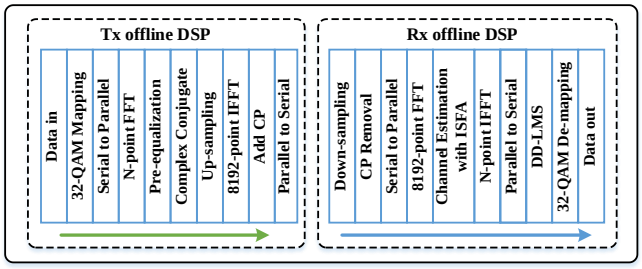

Fig. 4. Block diagram of DFT-S DMT system.

III. Experimental Setup

The experimental setup for the 32-QAM DFT-S DMT signal transmission over 1km SSMF in an IM/DD system is shown in Fig. 5. The baseband signal is generated off-line in Matlab and uploaded into a DAC with a sampling rate of 80-GSa/s and 3 dB bandwidth of 20-GHz.

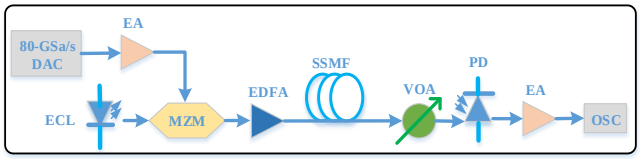

Fig. 5. Experimental setup for the DFT-S DMT signal transmission in IM-DD system. ECL: external cavity laser, EA: electrical amplifier, MZM: Mach-Zehnder modulator, VOA: variable optical attenuator, PD: photo detector, OSC: oscilloscope.

An external-cavity laser (ECL) with the center wavelength of 1552nm is used as a carrier source. The electrical signals generated from the DAC are amplified and fed into a Mach-Zehnder modulator (MZM) with 30-GHz 3 dB bandwidth. After amplified by the Erbium-doped fiber amplifier (EDFA), signals are coupled into 1 km SSMF. After fiber transmission, the optical power for measurement is adjusted by a variable optical attenuator (VOA). The received optical signal is detected by a photodetector (PD) with 45-GHz bandwidth to achieve optical-to-electrical conversion. Finally, the amplified electrical signals are sent into a digital storage oscilloscope with 100-GSa/s sample rate and 33-GHz electrical bandwidth.

IV. Experimental Results and Discussions

Since GS-32-QAM and PS-32-QAM can be proved to obtain the shaping gain over an AWGN channel, we have to verify the noise distribution in the IM/DD system. We measure the noise distribution of received uniform 32-QAM signals in the IM/DD system by calculating the symbol probability density functions (PDFs). Fig. 6 shows the measured PDFs of the normalized signals after transmission. A Gaussian curve is also plotted in Fig. 6 with the same mean and standard deviation of the measured signals for comparison. It can be observed that the noise distribution of the received signals is nearly Gaussian distribution. Therefore, this short-reach IM/DD channel can be well approximated by an AWGN channel, which justifies the application of GS-32-QAM and PS-32-QAM.

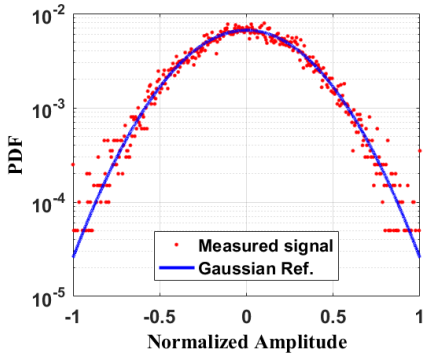

Fig. 6. Measured PDFs of the normalized signals after transmission.

A. Comparison in the low SNR Case

We need to keep the same transmission rate when we compare the performance of GS-32-QAM, PS-32-QAM and uniform 32-QAM in the experiment. Therefore, the code rate of GS-32-QAM and uniform 32-QAM should be 4/5 when the code rate of PS-32-QAM is 9/10. Then, the transmission rates of three 32-QAM formats are all 4 b/s.

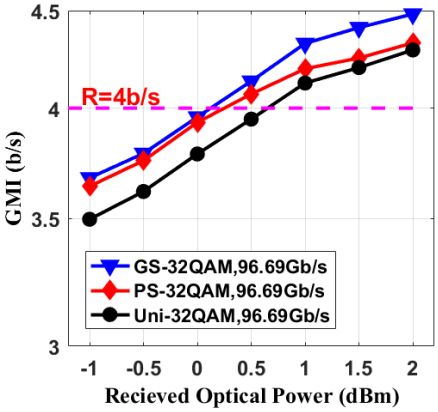

Fig. 7. Measured GMI versus received optical power with 96.69-Gb/s net bit rate.

We first experimentally compare the GMI performance of three 32-QAM formats with the same net bit rate in the low SNR case, where the signal bandwidth is wider than 3 dB bandwidth of DAC and the SNR degrades due to the roll-off effect of DAC. As mentioned before, when the signal bandwidth is 25-GHz, the net bit rate is thus 96.69-Gb/s. Fig. 7

shows the measured GMI of three 32-QAM formats versus received optical power after 1-km SSMF transmission with 96.69-Gb/s net bit rate. The horizontal dashed line indicates the same transmission rate for different 32-QAM formats, whose crossing points with the measured GMI curves determine the required received optical power for error free decoding without considering any implementation penalty for the FEC. The GMI performance of GS-32-QAM is even better than PS-32-QAM under the same received optical power. Take the case of uniform 32-QAM as a reference, the receiver sensitivity improvement for PS-32-QAM is 0.4 dB at the GMI threshold of 4b/s, while it is 0.5 dB for GS-32-QAM with the net bit rate of 96.69-Gb/s.

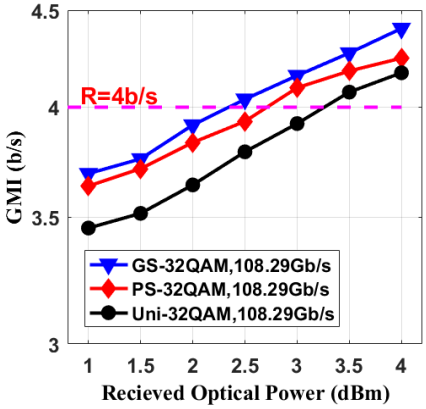

Fig. 8. Measured GMI versus received optical power with 108.29-Gb/s net bit rate.

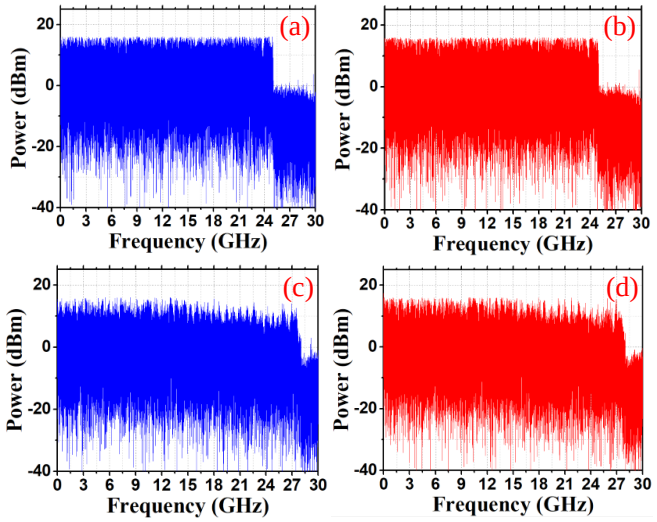

Fig. 9. Electrical spectra of the received GS-32-QAM DMT and PS-32-QAM DMT signals with 25- and 28-GHz bandwidth.

For the transmitted signals with bandwidth up to 28-GHz, the corresponding net bit rate is 28×4×8192/ (8192+16) ×31/32=108.29-Gb/s. In Fig. 8, the GMI performance of three mapping formats degrades with the increase of transmission bandwidth, but it is still above GMI threshold when the received optical power is no less than 3 dBm. GS constellation still obtains no less than 0.2 b/s GMI gain with respect to uniform 32-QAM constellation under different received optical power. Meanwhile, GS-32-QAM obtains around 0.9 dB receiver sensitivity gain while the receiver sensitivity gain of PS-32-QAM is 0.6 dB compared with uniform 32-QAM at the GMI threshold of 4b/s. It is worth noting that the gap between GS-32-QAM and PS-32-QAM increases from 0.1 to 0.3 dB with the increase of bandwidth which indicates the superiority of GS constellation applied in the low SNR case.

Figs. 9(a) and 8(b) give the electrical spectra of the received GS-32-QAM and PS-32-QAM DMT with 25-GHz bandwidth, respectively. Figs. 9(c) and 8(d) show the electrical spectra of the received GS-32-QAM and PS-32-QAM DMT with 28-GHz bandwidth, respectively. The electrical spectrum is made flat with the implementation of pre-equalization.

As we know, after pre-equalization, more power is allocated in high frequency edge and experiences severe power fading. It will lead to more power loss after passing through the bandwidth-limited channel. Therefore, the total SNR decreases after pre-equalization. The shaping gain gap between probabilistic shaping and geometric shaping becomes small due to the reduced SNR. Moreover, the roll-off effect of DAC can introduce severe ISI. LDPC code is introduced to resist ISI and improve the system performance. To maintain the same net rate, the overhead (OH) of GS-32-QAM is larger than that of PS-32-QAM, which leads to higher coding gain and better robustness against serious ISI for GS-32-QAM. Therefore, GS-32-QAM outperforms PS-32-QAM in the low SNR case.

Moreover, we also compare GS-32-QAM with PS-64-QAM at the code rate of 4/5, so that the coding gain is the same. To maintain the same transmission rate, the entropy of PS-64-QAM should be 5.2 bits/symbol. As shown in Fig. 10, PS-64-QAM with Gray mapping obtains better shaping gain than GS-32-QAM. The receiver sensitivity gain gap between PS-64-QAM and GS-32-QAM is 0.3 dB at the net bit rate of 96.69-Gb/s, while it is 0.2 dB at the net bit rate of 108.29-Gb/s. Although PS-64-QAM with higher PAPR will influence the nonlinear performance, it still outperforms GS-32-QAM and PS-32-QAM with the best GMI performance in the bandwidth-limited IM-DD system.

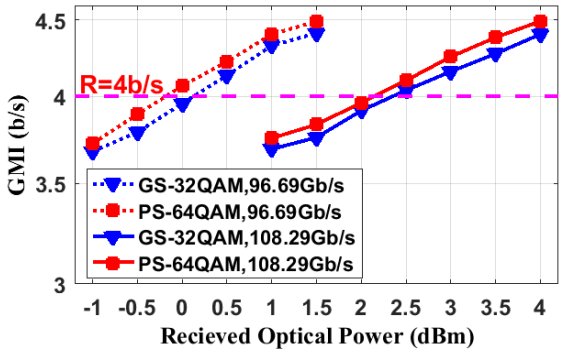

Fig. 10. Measured GMI versus received optical power for GS-32-QAM and PS-64-QAM with 96.69-Gb/s and 108.29-Gb/s net bit rates.

B. Comparison in the high SNR Case

We also experimentally compare the GMI performance of GS-32-QAM DMT and PS-32-QAM DMT in the high SNR case, where the signal bandwidth is narrower than 3 dB bandwidth of DAC and the SNR is relatively high. The GMI performance of GS-32-QAM and PS-32-QAM DMT with

15-GHz bandwidth at the same net data rate of 15×4×8192/ (8192+16) ×31/32=58.01-Gb/s is shown in Fig. 11. It suggests that the GMI performance of PS-32-QAM is better than GS-32-QAM. The required input power at the GMI threshold of 4b/s is -4.5, -4.2 and -4 dBm for PS-32-QAM, GS-32-QAM and uniform 32-QAM, respectively. Compared to uniformly distributed 32-QAM signal, PS-32-QAM can provide the receiver sensitivity gain of 0.5 dB while GS-32-QAM can provide the receiver sensitivity gain of 0.2 dB.

The experimental results of the comparison between GS-32-QAM and PS-32-QAM DMT with 18-GHz bandwidth at the same net bit rate of 18×4×8192/ (8192+16) ×31/32=69.61-Gb/s are given in Fig. 12. PS-32-QAM still outperforms GS-32-QAM in the high SNR case. The required input power at the GMI threshold of 4b/s is -3, -2.9 and -2.5 dBm for PS-32-QAM, GS-32-QAM and uniform 32-QAM, respectively. The receiver sensitivity gain for PS-32-QAM is 0.5 dB while the receiver sensitivity gain for GS-32-QAM is 0.4 dB. It suggests that the gap between PS-32-QAM and GS-32-QAM is narrowed from 0.3 to 0.1 dB with the increase of bandwidth. As a result, it indicates that PS-32-QAM outperforms GS-32-QAM in the high SNR case.

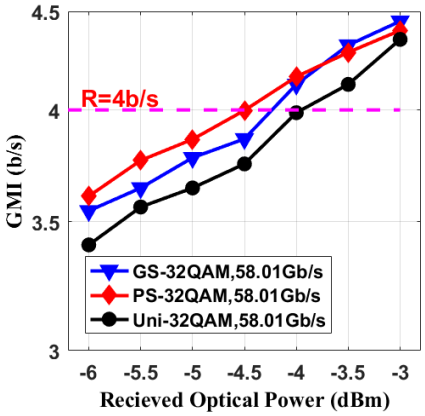

Fig. 11. Measured GMI versus received optical power with 58.01-Gb/s net bit rate.

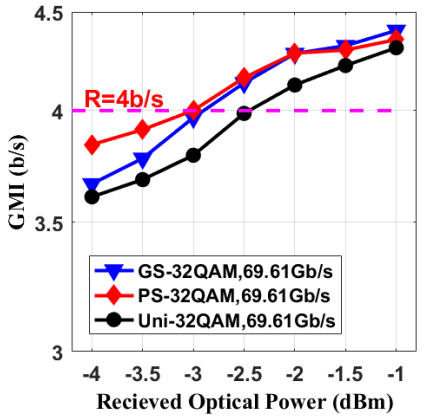

Fig. 12. Measured GMI versus received optical power with 69.61-Gb/s net bit rate.

V. Conclusion

We have investigated the transmission performance of the 32-QAM DFT-S DMT signal and conducted the comparison of the performance of GS and PS constellations with regular square QAM format in both low SNR and high SNR cases. According to our analysis, the proposed GS-32-QAM constellation outperforms PS-32-QAM in terms of computation complexity and receiver sensitivity in low SNR scenario. However, PS-32-QAM has better receiver sensitivity than GS-32-QAM and the gap between PS-32-QAM and GS-32-QAM is negligible in the high SNR case.

References

[1] T. Fehenberger, A. Alvarado, G. Böcherer, et al, "On probabilistic shaping of quadrature amplitude modulation for the nonlinear fiber channel," *J. Light. Technol.*, vol. 34, no. 21, pp. 5063–5073, 2016.

[2] B. Liu, et al, "Probabilistic shaping for ROF system with heterodyne coherent detection," *APL Photonics*, vol. 2, no. 5, 056104, 2017.

[3] F. Steiner, P. Schulte, and G. Böcherer, "Approaching waterfilling capacity of parallel channels by higher order modulation and probabilistic amplitude shaping," *IEEE Conference on Information Sciences and Systems (CISS)*, no. Dm, 2018.

[4] J. Cho, X. Chen, S. Chandrasekhar, G. Raybon, R. Dar, L. Schmalen, E. Burrows, A. Adamiecki, S. Corteselli, Y. Pan, D. Correa, B. McKay, S. Zsigmond, P. J. Winzer, and S. Grubb, "Trans-Atlantic field trial using high spectral efficiency probabilistically shaped 64-QAM and single carrier real-time 250-Gb/s 16-QAM," *J. Light. Technol.*, vol. 36, no. 1, pp. 103–113, 2018.

[5] A. Ghazisaeidi, I. F. d. J. Ruiz, R. R.-Muller, L. Schmalen, P. Tran, P. Brindel, A. C. Meseguer, Q. Hu, F. Buchali, G. Charlet, and J. Renaudier, "65Tb/s transoceanic transmission using probabilistically-shaped PDM-64QAM," in *Proc. Eur. Conf. Opt. Commun.*, Dusseldorf, Germany, Sep. 2016, Paper Th.3.C.4.

[6] P. Schulte and G. Böcherer, "Constant composition distribution matching," *IEEE Trans. Inform. Theory*, vol. 62, no. 1, pp. 430–434, 2016.

[7] F. Buchali, F. Steiner, G. Böcherer, L. Schmalen, P. Schulte, and W. Idler, "Rate adaptation and reach increase by probabilistically shaped 64-QAM: An experimental demonstration," *J. Light. Technol.*, vol. 34, no. 7, pp. 1599–1609, 2016.

[8] F. Buchali, G. Böcherer, W. Idler, L. Schmalen, P. Schulte, and F. Steiner, "Experimental demonstration of capacity increase and rate-adaptation by probabilistically shaped 64-QAM," presented at the *European Conf. Optical Communication*, Valencia, Spain, Sep. 2015, Paper PDP.3.4.

[9] F. Jardel, et al.," Experimental comparison of 64-QAM and combined geometric-probabilistic shaped 64-QAM", presented at the *European Conf. Optical Communication*, Gothenburg, 2017.

[10] Z. Qu and I. B. Djordjevic, "Geometrically shaped 16QAM outperforming probabilistically shaped 16QAM," presented at the *European Conf. Optical Communication*, Gothenburg, 2017.

[11] B. F. Beidas, et al., "Faster-than-Nyquist signaling and optimized signal constellation for high spectral efficiency communications in nonlinear satellite systems", *IEEE Military Communications Conference*, 2014.

[12] H. Méric, et al., "Approaching the Gaussian channel capacity with APSK constellations", *IEEE Communications Letters*, vol. 19, no. 7, pp. 1125-1128, 2015.

[13] N. S. Loghin, J. Zöllner, B. Mouhouche, D. Ansorregui, J. Kim, and S. I. Park, "Non-uniform constellations for ATSC 3.0," *IEEE Trans.Broadcast.*, vol. 62, no. 1, pp. 197–203, Mar. 2016

[14] B. Moore, G. Takahara, F. Alajaji, "Pairwise optimization of modulation constellations for non-uniform sources," *Canadian Journal of Electrical and Computer Engineering*, vol. 34, no. 4, pp.167-177, 2009.

[15] S. Zhang, F. Yaman, E. Mateo, et al, "A generalized pairwise optimization for designing multi-dimensional modulation formats," in *Proc. 2017Opt. Fiber Commun. Conf. Exhib.*, Mar. 2017, pp. 1–3.

[16] T. Koike-Akino, D. S. Millar, K. Parsons, and K. Kojima, "GMI-maximizing constellation design with Grassmann projection for parametric shaping," in *Proc. 2016 Opt. Fiber Commun. Conf. Exhib.*, Mar. 2016, pp. 1–3.

[17] S. Zhang et al., "50.962Tb/s over 11185 km Bi-directional C + L transmission using optimized 32-QAM," in *Conference on Lasers and Electro Optics*. Optical Society of America, 2017, Paper JTh5A.9.

[18] T. Liu, et al., "On the optimum signal constellation design for high-speed optical transport networks", *Optics Express*, vol. 20, no. 18, pp. 20396-406, 2012.

[19] A. Pilipetskii, C. Davidson, et al., "70.4 Tb/s capacity over 7,600 km in C+L band using coded modulation with hybrid constellation shaping and nonlinearity compensation", in *Proc. 2017Opt. Fiber Commun. Conf. Exhib.*, Mar. 2017, pp. 1–3.

[20] F. Steiner and G. Bocherer, "Comparison of geometric and probabilistic ¨ shaping with application to ATSC 3.0," in *Int. ITG Conf. Source Channel Coding*, Hamburg, Germany, Feb. 2017.

[21] D. S. Millar, T. Fehenberger, et al, "Coded modulation for next-generation optical communications," in *Proc. 2018Opt. Fiber Commun. Conf. Exhib.*, Mar. 2018, pp. 1–3.

[22] L. Zhang, T. Zuo, Y. Mao, Q. Zhang, E. Zhou, G. N. Liu, and X. Xu, "Beyond 100-Gb/s transmission over 80-km SMF using direct-detection SSB-DMT at C-band," *J. Light. Technol.*, vol. 34, no. 2, pp. 723–729, 2016.

[23] J. Shi, J. Zhang, Y. Zhou, Y. Wang, N. Chi, and J. Yu, "Transmission performance comparison for 100Gb/s PAM-4, CAP-16 and DFT-spread OFDM with direct detection," *J. Light. Technol.*, vol. 35, no. 23, pp. 5127–5133, 2017.

[24] D. Zou, Y. Chen, F. Li, Z. Li, Y. Sun, L. Ding, J. Li, Yi, X. Yi, L. Li, and Z. Li, "Comparison of bit-loading DMT and pre-equalized DFT-spread DMT for 2-km optical interconnect system," *J. Light. Technol.*, vol. 37, no. 10, pp. 2194–2200, 2019.

[25] Z. Qu, S. Zhang, and I. B. Djordjevic, "Universal hybrid probabilistic-geometric shaping based on two-dimensional distribution matchers", in *Proc. 2018Opt. Fiber Commun. Conf. Exhib.*, Mar. 2018, pp. 1–3.